

Vacancy Induced Splitting of Dirac Nodal Point in Graphene

W. Zhu¹, W. Li^{1*}, Q. W. Shi¹, X. R. Wang^{2,3*}, X. P. Wang¹, J. L. Yang¹, J. G. Hou¹

¹*Hefei National Laboratory for Physical Sciences at Microscale,
University of Science and Technology of China, Hefei 230026, China*

²*Department of Physics, The Hong Kong University of Science and Technology, Clear Water Bay, Kowloon, Hong Kong and*

³*School of Physics, Shandong University, Jinan, P. R. China**

(Dated: November 8, 2021)

We investigate the vacancy effects on quasiparticle band structure of graphene near the Dirac point. It is found that each Dirac nodal point splits into two new nodal points due to the coherent scattering among vacancies. The splitting energy between the two nodal points is proportional to the square root of vacancy concentration. In addition, an extra dispersionless impurity band of zero energy due to particle-hole symmetry is found. Our theory offers an excellent explanation to the recent experiments.

PACS numbers: 81.05.Uw, 71.55.-i, 71.23.-k

One of the important features of pristine graphene is the Dirac nodal structures centered at two inequivalent corners K and K' of the first Brillouin zone with linear energy dispersion [1, 2]. The common belief is that the Dirac nodal structure is robust against the short-ranged potential scattering because the Fermi wavelength diverges at the Dirac nodal point and the electronic state correction due to the scatters is negligible [3]. However, the recent progresses in the classical wave physics demonstrates that local resonant structures can dramatically modify waves whose wavelengths are several orders of magnitude larger than the structure sizes [4–6]. Vacancies as well as various chemical adsorbates in graphene can create resonant states in the vicinity of the Dirac point. An effect analogous to the classical wave is expected. Those locally resonant states should dramatically change the graphene electronic structures and transport properties near the Dirac nodal point. Indeed, the angle-resolved photoemission spectroscopy (ARPES) indicates the opening of a tunable band gap near the Dirac point and the formation of a dispersionless impurity band in hydrogenated quasi-free-standing graphene [7, 8]. Another study of hydrogenated graphene on SiC showed signals of a metal-to-insulator transition (MIT) due to the electron localization [9]. Away from the charge neutrality point, the transport measurements demonstrated a sub-linear carrier dependence of the conductivity [10]. Within the Boltzmann transport framework, a sublinear conductivity in charge density was predicted [11]. Away from the Dirac nodal point, this theoretical prediction agrees well with experiments. However, it fails to explain the transport behavior near the nodal point, which is supposed due to the breakdown of Boltzmann transport theory there [12, 13]. Nevertheless, those predictions have not included the influence from the substantial change of electronic structure arising from the resonant scattering. In fact, numerical simulations show that a dramatic change in the density of states (DOS) occurs near the nodal point [14, 15]. Therefore, a deep understanding of

the resonant scattering effects is needed.

In this letter, we present a calculation on the effects of the vacancy resonant scattering on Dirac nodal structure in graphene. The quasiparticle dispersion is extracted from the spectral function $A(\mathbf{k}, E)$ which can be calculated by extending the well developed Lanczos approach [16]. In contrast to the previous theoretical studies of the spectral function by the average T-matrix approximation (ATA) [17–19] or the self-consistent T-matrix approximation (SCTA) [17, 20], our proposed method is more general and nonperturbative, including all the coherent multiple scattering contributions. The ATA considers only the averaged contribution of impurity potentials without interference effect from different impurities while the SCTA includes the partial contribution from quantum interference. We found that, instead of only one peak in the spectral function for a given momentum in the case of a weak short-range scattering [16], the resonant scattering yields multi-peaks in the spectral function. This leads to a complete change of quasiparticle band structure. Each Dirac nodal point splits into two new nodal points and the splitting energy between the two nodal points is proportional to the square root of vacancy concentration. In addition, an extra dispersionless impurity band is developed at zero energy. The fact that we can obtain this existing band proves the accuracy of our method. Our results also suggest that the Boltzmann theory could work well near the Dirac point if the modified energy dispersion is taken into account.

π -electrons of pristine graphene can be modeled by a tight-binding Hamiltonian on a honeycomb lattice of two sites per unit cell, $H_0 = t \sum_{\langle ij \rangle} |i\rangle \langle j| + h.c.$, where t is the hopping energy between the nearest neighboring atoms. We consider vacancy disorder potential V in this work because it gives rise to the resonant scattering which may also arise from hydrogen or fluorine adsorbates [21]. Vacancies are introduced by randomly removing lattice sites with probability n_{imp} (vacancy concentration). In the presence of a disorder potential V , the single electron

properties can be obtained from the ensemble-averaged Green function $G(\mathbf{k}\pm, E) = \langle \mathbf{k}\pm | \frac{1}{E+i\eta-H_0-V} | \mathbf{k}\pm \rangle$, where $|\mathbf{k}\pm\rangle$ is eigenstate of H_0 . This Green function can be obtained numerically by using the Lanczos recursive method [15, 16, 22–24]. To numerically obtain an exact ensemble-averaged Green's function near the Dirac point, a large lattice containing millions sites (4800×4800) is used. The large samples guarantee that the calculated Green's function is free from the finite size errors. In the following calculations, the broadening parameter is set to be $\eta = 0.001t$ [16].

Self-energy function Σ is defined in the Dyson's equation as $G(\mathbf{k}, E) = G_0(\mathbf{k}, E) + G_0(\mathbf{k}, E)\Sigma(\mathbf{k}, E)G(\mathbf{k}, E)$. Thus one has $\Sigma(\mathbf{k}, E) = G_0^{-1}(\mathbf{k}, E) - G^{-1}(\mathbf{k}, E)$ [25, 26]. Fig. 1 is the energy-dependence of calculated real (a) and imaginary (b) parts of the self-energy function in the conduction band for various momenta $k = 0, 0.021$ and 0.042 along $K - M$ direction in the Brillouin zone. To have a visible effect of the resonant scattering, a relatively large vacancy concentration $n_{imp} = 0.1\%$ is used in the calculation. Within energy range of $[-0.02t, 0.02t]$ (depending on the vacancy concentration), both $Re\Sigma$ and $Im\Sigma$ depend explicitly on the momentum, as shown in Fig. 1(c-d). This momentum dependence of the self-energy results in the failure of the ATA or SCTA [27]. It also shows that the effective homogeneous medium approximation is invalid around the Dirac point. Beyond this energy range, however, our simulations show insensitiveness of the self-energy function to wave vector \mathbf{k} , and Σ varies only with the energy. More interestingly, a spike in $Re\Sigma$ around the Dirac point is observed in Fig. 1(c), in contrast with the ATA and SCTA [17, 20]. Another notable feature is that the ATA predicts a peak of $Im\Sigma$ at the Dirac point. Instead, a dip at the Dirac point (Fig. 1(d)) is observed. Though the self-energy function shows a complicated momentum and energy dependence around the Dirac point, we find that it still satisfies the Kramers-Kronig relation [26]. In order to have a better picture of the quasiparticles of the system, we compute the spectral function below.

The single-particle spectral function relates to the Green's function through $A(\mathbf{k}\pm, E) = -ImG(\mathbf{k}\pm, E)/\pi$ [26]. Generally speaking, the spectral function $A_0(\mathbf{k}, E)$ is a δ -function in the absence of disorders, reflecting that the wave vector \mathbf{k} is a good quantum number and all its weight ratio is precisely at energy $E = E_{\mathbf{k}\pm}$. In the presence of disorders, the δ -peak is broadened due to finite life time of quasiparticles, resulting from the disorder scattering effect. The linewidth of the peak is given by $Im\Sigma(E)$ that measures the elastic relaxation lifetime τ_e , $\tau_e = \frac{\hbar}{-2Im\Sigma(E)}$. These general features are indeed observed in the weak scattering cases [16]. The spectral function is qualitatively different in the strongly resonant scattering regime. Taking $A(k = 0+, E)$ in Fig. 2(a) as an example, the spectral function is surprisingly split into

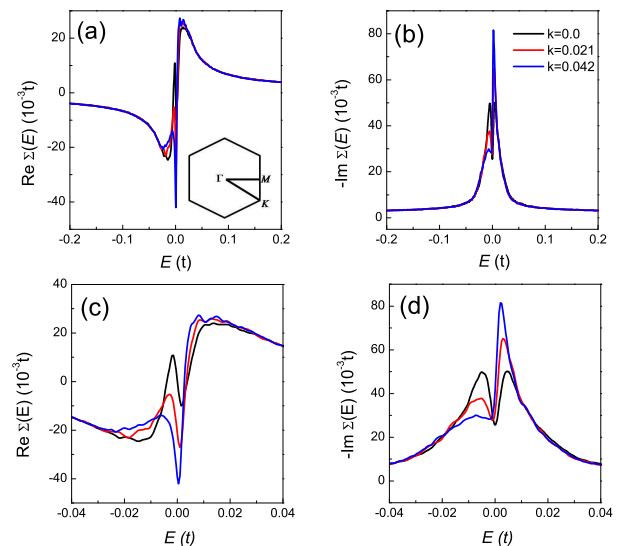


FIG. 1: (Color online) Real (a) and imaginary (b) parts of self-energy function Σ as a function of energy E for various wave vectors: $k = 0$ (black), 0.021 (red) and 0.042 (blue) (in unit of $1/a$). The wave vector varies from the K point to M point in the Brillouin zone (Inset of (a)). (c) and (d) are the enlarged views of (a) and (b) near the Dirac point ($E = 0$).

three peaks: One broadened peak (p_-) centering in the hole regime ($E < 0$), one broadened peak (p_+) centering in the electron regime ($E > 0$) and one sharp peak (p_0) at charge neutrality point ($E = 0$). The p_- peak moves toward $E = 0$ as the wave vector \mathbf{k} increases while its height is reduced and its width increases. p_0 peak position do not change with \mathbf{k} while its height decreases with \mathbf{k} . Meanwhile, the p_+ peak moves away from $E = 0$ and its height is significantly increased and its width is narrowed. When the wave vector exceeds a threshold value, the p_- and the p_0 peaks disappear.

By tracing the trajectories of the peaks of the density plot of spectral function $A(\mathbf{k}, E) = A(\mathbf{k}+, E) + A(\mathbf{k}-, E)$ in the $k - E$ plane, shown in Fig. 2(b), one can obtain the dispersion relation $E(\mathbf{k})$ shown in Fig. 2(c). Many other physical quantities like the group velocity and elastic scattering time can be directly extracted from Fig. 2(b-c). Away from the Dirac point, the p_+ peak dominates the spectral function and the effective energy dispersion approaches the linear behavior (red square dotted line). Around the Dirac point, Fig. 2(b) clearly shows the anomalous band structure of quasiparticle. The dispersionless impurity band (green diamond dotted line) corresponding to the p_0 peak in the spectral function indicates the localized states relating to the kink in $Re\Sigma$ and the dip in $Im\Sigma$. The existence of these localized states are originated and protected by the particle-hole symmetry [28]: Each vacancy deducts one level from the continue band, and at the same time pulls out another level from the continue band to a highly localized zero energy state (hopping is not allowed in order to be dispersionless)

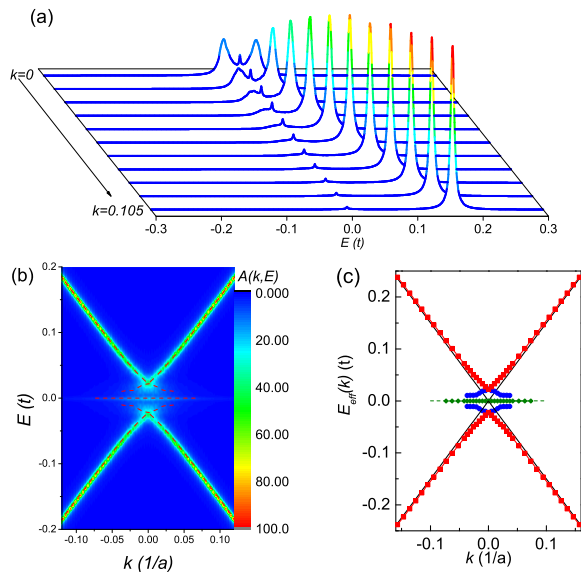


FIG. 2: (Color online) (a) Quasiparticle spectral function $A(\mathbf{k}+, E)$ plotted as a function of energy E for various wave vectors at vacancy concentration $n_{imp} = 0.1\%$. $A(\mathbf{k}-, E)$ can be obtained by reflecting $A(\mathbf{k}+, E)$ around $E = 0$ due to the particle-hole symmetry. (b) Density plot of spectral function $A(\mathbf{k}, E) = A(\mathbf{k}+, E) + A(\mathbf{k}-, E)$ in $\mathbf{k} - E$ plane for $n_{imp} = 0.1\%$. (c) Dispersion relation (dotted line) extracted from (b). The blue circles and green diamonds are the new resonant band and dispersionless impurity band, respectively. For comparison, the linear dispersion of clean graphene is plotted as the black solid lines.

[29]. Using the exact diagonalization method, one can also see from the inverse participation ratio analysis that these impurity states are highly localized around each vacancy [14]. Applying the Stoner theory for magnetism, this zero-bandwidth dispersionless band may lead to ferromagnetism for the system when the electron-electron interaction is switched on. This observation is consistent with the recent experiment that directly confirms the dispersionless impurity band in graphene [8]. More importantly, a new dispersion quasiparticle band (blue circles) with finite lifetime corresponding to the p_- peak in the spectral function is observed in our calculations. This indicates that a splitting of host band of pristine graphene happens near the Dirac point.

The physical origin of above results comes from vacancy effect. Firstly, they create zero energy dispersionless impurity band, forming resonance scattering centers. The strong resonance scattering around the Dirac point where the electronic de Broglie wavelength λ is much bigger than the average vacancy-to-vacancy distance $L_v \sim 1/\sqrt{n_{imp}}$. The coherent scattering between the neighboring vacancies mix K and K' points [30] so that a band gap is opened at the Dirac point. This coupling between the resonant scatters results in the appearance of p_- and p_+ peaks for both $A(\mathbf{k}+, E)$ and

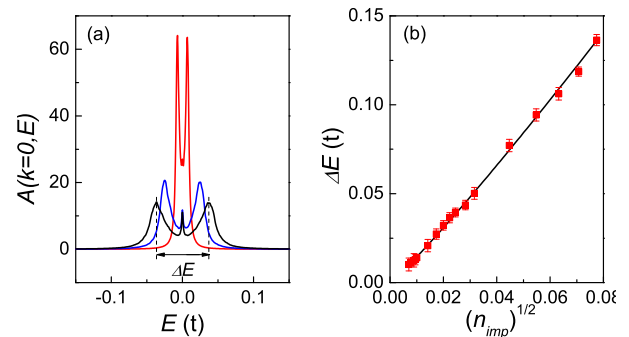


FIG. 3: (Color online) (a) Quasiparticle spectral function $A(\mathbf{k} = 0, E)$ as a function of energy E for several vacancy concentrations: $n_{imp} = 0.01\%$ (red), $n_{imp} = 0.1\%$ (blue), and $n_{imp} = 0.2\%$ (black). ΔE is the splitting energy between the two resonant peaks. (b) The vacancy concentration dependence of the splitting energy ΔE (red dots). The x-axis is in $(n_{imp})^{1/2}$. The black line is the linear fit $\Delta E = A(n_{imp})^{1/2}$ with $A = 1.76$.

$A(\mathbf{k}-, E)$. In fact, the direct evidence of the corresponding splitting of spectral function was indeed reported in hydrogenated graphene by ARPES [7, 8]. As the wave vector exceeds a threshold so that the wavelength is small $\lambda \ll L_v$, the quasiparticle is insensitive to the coupling of resonant states between neighboring vacancies in the low density. Hence, the new dispersive band disappears for the short wavelength. This is why ATA approximate approach works well far enough from the Dirac point.

Coming back to the spectral function at wave vector $\mathbf{k} = 0$ (as shown in Fig. 3(a)), one striking feature is the splitting energy ΔE (peak-to-peak distance between p_+ and p_- peaks). ΔE is the splitting energy between two nodal points at $\mathbf{k} = 0$ (neglecting the impurity band). The vacancy concentration dependence of ΔE is plotted in Fig. 3(b), where the x-axis is in the square root of n_{imp} that measures the inverse of vacancy-to-vacancy distance. The square root dependence of $\Delta E \propto \sqrt{n_{imp}} \propto 1/L_v$ supports the picture that the coherent scattering between vacancies play an important role.

The qualitative changes of the original linear dispersion relation around the Dirac point give rise to a completely different DOS near the zero energy. The DOS ρ can be directly computed from the spectral function by $\rho(E) = \frac{1}{N} \sum_k A(k, E)$. As shown in Fig. 4(a), a shape singular peak due to the dispersionless impurity band appears at $E = 0$. The smooth part of DOS has also a peak near $E = 0$ that is from the two extra dispersion relations (blue circles in Fig. 2c). The DOS far away from $E = 0$ are essentially from the original linear dispersion relation of pristine graphene. The width of the energy regime influenced by vacancies is approximately proportional to $\Delta E \sim \sqrt{n_{imp}}$. All of these results agree exactly with the previous numerical simulation [14, 15] and recent APRES experiment [8]. Thus, it proves that our

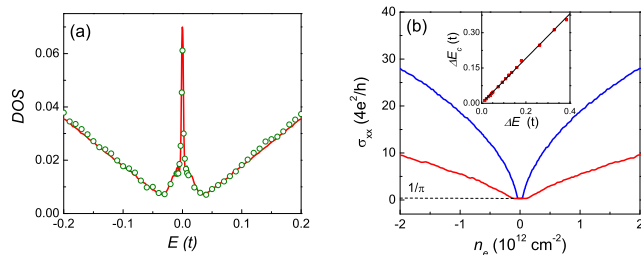


FIG. 4: (Color online) (a) Comparison of the DOS obtained from our spectral function (red line) with the numerical simulation of reference [15] (green dots) for $n_{imp} = 0.1\%$. Excellent agreement demonstrates the accuracy of our calculations. (b) Conductivity as a function of charge density n_e for $n_{imp} = 0.01\%$ (blue) and $n_{imp} = 0.1\%$ (red), respectively. Inset: The conductivity plateau width in terms of energy ΔE_c vs splitting energy ΔE shown in Fig. 3. ΔE_c can be obtained from the relationship $n_e = \int^{E_F} \rho(E) dE$. Black line is the linear fit of $\Delta E_c = A\Delta E$ with $A = 0.95$.

spectral analysis captures the correct physics near the Dirac point. Furthermore, it shows that ATA or SCTA fail to describe this interesting and important feature of DOS [17].

The new feature of DOS near the zero energy has important consequences in electron transport. To clearly see it, we calculate the conductivity by using the Kubo formula at zero temperature,

$$\sigma_{xx} = \frac{\hbar}{2\pi L^2} \overline{\text{Tr}[j_x G^R(E) j_x G^A(E)]}.$$

Neglect the corrections to current vertex and use the Drude-Boltzmann approximation $\overline{G^R G^A} \simeq \overline{G^R} \overline{G^A}$ [27], our calculated conductivity as a function of charge density for $n_{imp} = 0.01\%$ and 0.1% is plotted in Fig. 4(b). A plateau of conductivity $4e^2/\pi h$ is observed near the charge neutrality point. The width of the plateau increases with the vacancy concentration. Away from the plateau, the conductivity increases with charge density sublinearly. These results are consistent with those of the numerical real space calculations [13, 31, 32]. Interestingly, plateau width in terms of energy ΔE_c is almost equal to the splitting energy ΔE as shown in the inset of Fig. 4(b), which implies that the origin of the plateau is the anomalous band structure near the Dirac point. This conductivity plateau provides an interpretation to the experimental observation [33]. It should be pointed out that our calculations do not include the contribution from the impurity-band-induced variable range hopping conduction which may also be important in understanding the experiments at finite temperatures [8, 10].

In conclusion, we have studied vacancy induced resonant scattering effects on the one-electron properties of graphene. From our accurate spectral function, a new quasiparticle dispersion band due to the coherent scattering between neighbor vacancies is predicted, and

each Dirac point splits into two new nodal points. Furthermore, a dispersionless impurity band is developed at zero energy. This result sheds light on the characteristics of electronic structures and transport properties of graphene in the presence of resonant impurities.

This work is partially supported by NNSF of China (Nos. 10974187, 10874165), by NKBRP of China (No. 2011CB921403, No. 2012CB922003), and by KIP of the CAS (No. KJCX2-YW-W22). XRW acknowledges the support of Hong Kong RGC grants (#604109, RPC11SC05, and HKUST17/CRF/08).

* Electronic address: wliustc@mail.ustc.edu.cn; phxwan@ust.hk

- [1] K. S. Novoselov, *et. al*, Science **306**, 666(2004).
- [2] A. K. Geim, *et. al*, Nat. Mater. **6**, 183(2007).
- [3] K. Nomura, *et. al*, Phys. Rev. Lett. **98**, 076602(2006).
- [4] Z. Y. Liu, *et. al*, Science **289**, 1734(2000).
- [5] T. W. Ebbesen, *et. al*, Nature(London) **391**, 667(1998).
- [6] L. M. Moreno, *et. al*, Phys. Rev. Lett. **86**, 1114(2001).
- [7] D. Haberer, *et. al*, Nano Lett. **10**, 3360(2010).
- [8] D. Haberer, *et. al*, Phys. Rev. B **83**, 165433(2011).
- [9] A. Bostwick, *et. al*, Phys. Rev. Lett. **103**, 056404(2009).
- [10] J. H. Chen, *et. al*, Phys. Rev. Lett. **102**, 236805(2009).
- [11] T. Stauber, *et. al*, Phys. Rev. B **76**, 205423(2007).
- [12] J.P. Robinson, *et. al*, Phys. Rev. Lett. **101**, 196803(2008).
- [13] T. O. Wehling, *et. al*, Phys. Rev. Lett. **105**, 056802(2010).
- [14] V. M. Pereira, *et. al*, Phys. Rev. B **77**, 115109(2008).
- [15] S. D. Wu, *et. al*, Phys. Rev. B **77**, 195411(2008).
- [16] W. Zhu, *et. al*, Phys. Rev. B **82**, 153405(2008).
- [17] N. M. R. Peres, *et. al*, Phys. Rev. B **73**, 125411(2006).
- [18] S. S. Pershoguba, *et. al*, Phys. Rev. B **80**, 214201(2009); Y. V. Skrypnik, *et. al*, Phys. Rev. B **83**, 085421(2011); Y. V. Skrypnik, *et. al* arXiv-1105.4907.
- [19] M. Farjam, *et. al*, Phys. Rev. B, **83**, 193411(2011).
- [20] T. Lofwander, *et. al*, Phys. Rev. B **76**, 193401(2007).
- [21] S. Ihnatsenka, *et. al*, Phys. Rev. B **83**, 245442(2011).
- [22] J. K. Cullum and R. A. Willoughby, *Lanczos Algorithms for large symmetric eigenvalue problem*, (Birkhäuser, Boston, 1985).
- [23] E. Dagotto, Rev. Mod. Phys. **66**, 763(1994); L. C. Davis, Phys. Rev. B **28**, 6961(1983); B. Bauml, *et. al* *ibid.* **58**, 3663(1998); S. M. Anaage, *et. al*, *ibid.* **34**, 2336(1998).
- [24] L.-W. Wang, *et. al*, Phys. Rev. Lett. **80**, 4725(1997); Y. Zhang, *et. al*, Phys. Rev. Lett. **101**, 036403(2008).
- [25] E. N. Economou, *Green's Functions in Quantum Physics*, (Springer, New York, 2006).
- [26] A. Altland and B. Simons, *Condensed Matter Field Theory*, (Cambridge University Press, Cambridge, 2006).
- [27] E. Akkermans and G. Montambaux, *Mesoscopic physics of electrons and photons*, (Cambridge University Press, Cambridge, 2007).
- [28] A. H. Castro Neto, *et. al*, Rev. Mod. Phys. **81**, 109(2009).
- [29] Private communication with K. Yang.
- [30] Y. Y. Zhang, *et. al*, Phys. Rev. Lett. **102**, 106401(2009).
- [31] S. Yuan, *et. al*, Phys. Rev. B **82**, 115448(2010).
- [32] A. Ferreira, *et. al*, Phys. Rev. B **83**, 165402(2011).
- [33] Z. H. Ni, *et. al*, Nano. Lett. **10**, 3868(2010).